Thermal phase diagrams of columnar liquid crystals

G. Lamoureux, A. Caillé, and D. Sénéchal
Département de Physique and Centre de Recherche en Physique du Solide, Université de Sherbrooke, Sherbrooke, Québec, Canada J1K 2R1
(Received 8 January 1998)

In order to understand the possible sequence of transitions from the disordered columnar phase to the helical phase in hexa(hexylthio)triphenylene, we study a three-dimensional planar model with octupolar interactions inscribed on a triangular lattice of columns. We obtain thermal phase diagrams using a mean-field approximation and Monte Carlo simulations. These two approaches give similar results, namely, in the quasi-one-dimensional regime, as the temperature is lowered, the columns order with a linear polarization, whereas helical phases develop at lower temperatures. The helicity patterns of the helical phases are determined by the exact nature of the frustration in the system, itself related to the octupolar nature of the molecules.
[S1063-651X(98)04211-1]

PACS number(s): 61.30.Cz, 61.30.Gd, 64.70.Md

I. INTRODUCTION

The study of phase transitions in columnar liquid crystals [1,2] is of fundamental interest: These materials combine, aside from the vast phenomenology of soft matter, many features at the origin of important phenomena of the solid state. In particular, they show a relatively strong elastic anisotropy in the direction of the columns, a geometrical frustration of the intermolecular interaction coming from the triangular nature of the lattice of columns, and discoid molecules with nontrivial point-group symmetry. The present study is based on hexa(hexylthio)triphenylene (HHTT), whose discoid molecule is made of a rigid core of aromatic cycles and of six flexible hydrocarbon chains, responsible for its characteristic thermotropic character. HHTT is the only compound from the triphenylene derivatives to show two distinct columnar phases. Indeed, as the temperature decreases, the sequence of phases is the following: I (isotropic liquid), D_{hd} (disordered columnar phase), H (helically ordered columnar phase), and K (monoclinic crystal). These phases were identified by x-ray measurements on powders [3] and freely suspended strands [5–7] of HHTT.

These x-ray results are best interpreted by asserting that the D_{hd} phase of HHTT ($70\,^\circ\mathrm{C}<T<93\,^\circ\mathrm{C}$) has long-range positional order in the plane perpendicular to the columns: Columns are located on a triangular lattice. Within a column, short-range (liquid) positional order is realized. The columns slide freely one against the other. The H phase ($62\,^\circ\mathrm{C}<T<70\,^\circ\mathrm{C}$) has in-column positional and orientational helical order. In this last phase, two neighboring molecules in a single column are separated on the average by a distance $d_\parallel=3.6$ Å and rotated from each other by an angle $\alpha\approx 45°$, constant on the whole temperature interval of the phase. In order to reduce the frustration associated with the triangular geometry of the lattice, the lattice reorganizes itself in a superlattice $\sqrt{3}\times\sqrt{3}R30°$: One-third of the columns have a vertical offset of half the intermolecular distance ($d_\parallel/2$). The displaced columns have the opposite helicity: $\alpha\approx -45°$, instead of $+45°$. The x-ray experiments show long correlation lengths but, as proposed in [8], quasi-long-range order may be achieved. The nature of the in-column order in this phase is so far an open question and so is the exact mechanism of the $D_{hd}\leftrightarrow H$ transition. However, in this paper we will study solely the nature of *orientational* ordering of the HHTT molecules. We make the hypothesis that orientational ordering is robust with respect to the type of positional order (long-range vs quasi-long-range). This hypothesis is justified since, even in the case of quasi-long-range order, the positional coherence length is long enough that we may assume from the start that the molecules occupy well-defined positions (this also simplifies the mathematical treatment). It is thus possible to have orientational ordering even if the positional ordering is not long ranged. Indeed, as mentioned in Ref. [8], this underlying orientational order may very well favor quasi-long-range positional order along the columns. Thus the eventuality of quasi-long-range order makes the present work that much more relevant and interesting.

We suggest an effective Hamiltonian for the in-plane orientation of the HHTT molecules and study its thermal phase diagram by means of (i) a Landau free-energy functional in a mean-field approximation and (ii) Monte Carlo simulations on a finite-size lattice. Previous work has been done on the ground state of a related model [9] and on thermal phase diagrams for a two-dimensional model of uniform columns [10,11]. Our analysis confirms that, as previously seen at $T=0$, the octupolar G coupling [12] is determinative for obtaining the helicity configuration of the columns at any temperature. It also suggests that a variety of phases survive at $T\neq 0$. For weak transverse couplings, the model produces the expected low-temperature helical phases, but also suggests that some linearly polarized phases could exist at higher temperatures.

In Sec. II, the model Hamiltonian is presented with an emphasis on the intercolumn intermolecular interactions. In Sec. III the location of second-order phase transitions from the disordered phase to an ordred phase is obtained by a mean-field approach. It is followed by the construction of the thermal phase diagrams and characterization of the different phases in terms of the helicity pattern and relative orientation. In Sec. IV the thermal phase diagrams are obtained using Monte Carlo simulations on finite-size systems, in con-

 © 1998 The American Physical Society

junction with the spiraling algorithm. Finally, in Sec. V we discuss the results and conclude.

II. MODEL HAMILTONIAN

As indicated above, the main purpose of our calculation is to elucidate the role played by the angular degrees of freedom. Despite our ignorance of the exact nature of the positional order in the columns, we will freeze the positional degrees of freedom. A model for discotic phases allowing lattice distortions is studied in [4]. We also assume that the molecules lie on a three-dimensional triangular lattice of ordered columns, with one-third of the columns offset vertically. This simplification is certainly valid in the H phase, even if only quasi-long-range positional order existed, since order would then be maintained over many intermolecular distances. Accordingly, we will use (i,j) site indices to identify the unit cell of the three columns of the two-dimensional $\sqrt{3}\times\sqrt{3}R30°$ superlattice of columns and μ to identify the column: $\mu=1$ and 2 label the undisplaced columns and $\mu=3$ labels the columns offset by $d_{\parallel}/2$. Finally, an index k identifies the sites a molecule occupies in the (μ,i,j) column. We formally write (i,j,k) as m, an index labeling a plaquette of three molecules.

Within the framework of this plastic state model, each molecule (μ,m) has a well-defined position $\mathbf{r}_{\mu m}$ and an orientation labeled $\theta_{\mu m}$: We assume from the start that its plane is perpendicular to the direction of the columns. Orientational disorder may mimic an effective D_{hd} phase, which, however, would possess orientational and positional disorder along the columns. We did not explicitly consider the shape and flexibility of the tails, which would vary with the temperature. However, it has been suggested [5,6] that the stiffening of the tails may be responsible for the $D_{hd}\rightarrow H$ transition. The above considerations are implicitly integrated out as weakly temperature-dependent renormalization effects of the intercolumn interactions, allowing us to use, to a good approximation, an effective model with athermal values of the interaction parameters. The resulting thermal phase diagrams will represent a somewhat distorted version of the true temperature dependence.

The last thing to consider in the model is that the molecules are not exactly disklike: They develop a spontaneous chirality associated with the alternate arrangement of the aliphatic tails. Indeed, conformational analysis on compounds similar to HHTT [13,14] shows that this ''propeller blade'' configuration is the ground state of a single molecule and of two stacked molecules, one on top of the other.

A. Intracolumn interactions

In their ground state, two stacked HHTT molecules minimize their conformation energy by allowing an angular shift α between the two molecules [13,14]. An intrinsic chiral model represented by the Hamiltonian

$$-J\cos[3(\theta_{k+1}-\theta_k-\alpha)] \tag{1}$$

would be appropriate to represent this situation since the HHTT molecules have D_3 symmetry [15]. However, there is no *a priori* selection between right- and left-handed chiralities. In order to allow for the two possible chiralities of each column (the sign of α), we use a next-nearest-neighbor model (see [16–18]), with competing interactions of the form

$$-J_1\cos[3(\theta_{k+1}-\theta_k)]-J_2\cos[3(\theta_{k+2}-\theta_k)], \tag{2}$$

with $J_1>0$ and $J_2<0$. In the ground state, the molecules adopt a helical configuration with intrinsic pitch α, given by $\cos 3\alpha=-J_1/4J_2$ if $4|J_2|\geqslant|J_1|$ and zero otherwise. The J_1/J_2 ratio determines the magnitude of α, but allows opposite helicities for different columns and even helicity reversals within a column, separating helicity domains.

For an isolated molecule of HHTT at finite temperature, it is unclear whether chirality is a well-defined property: A conformation analysis [13] shows that the energy barrier between opposite chirality configurations is comparable to the thermal energy in the H and D_{hd} phases. In the present model, the chirality of a molecule is the result of a collective behavior governed by the intracolumn interactions (2): Every molecule in a particular helicity domain has the same chirality.

B. Intercolumn interactions

Given the approximation that each molecule is fully described by its orientation $\theta_{\mu m}$, we may write its mass density as a multipole expansion [12,19]. Because of the D_3 point symmetry of the molecule, the first nonzero moment is the octupolar moment, which may be represented by Q_{klm}, a rank-three tensor $(k,l,m=x,y)$. The only interactions that are bilinear in Q as well as invariant with respect to the symmetries of the hexagonal lattice have a $\cos 3(\theta-\theta')$ or $\cos 3(\theta+\theta')$ form [12]. The intercolumn interaction is then approximated to be

$$-J\cos[3(\theta_{\mu ij}-\theta_{\mu' i' j'})]-G\cos[3(\theta_{\mu ij}+\theta_{\mu' i' j'})]. \tag{3}$$

The first term is invariant under continuous rotations and would be present even if the molecules had lower symmetry multipole moments. However, the second term is specific to the octupolar character of the molecules and has only a discrete rotational symmetry.

To extract the D_3 symmetry of the molecules, we replace the real orientations $\theta_{\mu m}$ by angular variables $\phi_{\mu m}=3\theta_{\mu m}$. The complete Hamiltonian of the system then reads

$$H=-\sum_{\mu,\nu}\sum_{m,n}[J_{\mu m,\nu n}\cos(\phi_{\mu m}-\phi_{\nu n}) + G_{\mu m,\nu n}\cos(\phi_{\mu m}+\phi_{\nu n})]. \tag{4}$$

$J_{\mu m,\nu n}$ contains the intracolumn interactions: Each site is coupled to its first and second intracolumn nearest neighbors by J_1 and J_2 as in Eq. (2). The intercolumn couplings are embedded in $J_{\mu m,\nu n}$ and $G_{\mu m,\nu n}$. Each $\mu=1$ site interacts with three $\mu=2$ and six $\mu=3$ neighbors (three upward and three downward). The intercolumn couplings have different values: J and G for in-plane molecules (1-2 bonds) and J' and G' for out-of-plane molecules (1-3 and 2-3 bonds) [see Fig. 1(b)]. Nevertheless, it is physically justified [10] to sup-

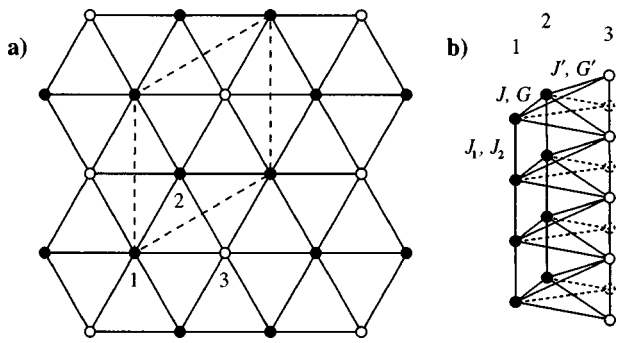

FIG. 1. (a) Two-dimensional triangular lattice of columns. Open circles represent displaced columns ($\mu=3$) and closed circles undisplaced columns ($\mu=1$ and 2). Dashed lines represent the unit cell of the superlattice. (b) Three-dimensional illustration of the couplings for three columns. Dotted lines represent fictitious sites and interactions for an undisplaced column 3.

pose that $J'\approx J$ and $G'\approx G$ and, for simplicity, we assume $J'=J$ and $G'=G$. J_1 is positive and taken to be unity (it sets the energy scale).

With the notations

$$c_{\mu m}=\cos(\phi_{\mu m}),\quad s_{\mu m}=\sin(\phi_{\mu m}), \tag{5}$$

we may rewrite the Hamiltonian (4) as

$$H=-\sum_{\mu,\nu}\sum_{m,n}[J^c_{\mu m,\nu n}c_{\mu m}c_{\nu n}+J^s_{\mu m,\nu n}s_{\mu m}s_{\nu n}], \tag{6}$$

where $J^c_{\mu m,\nu n}=J_{\mu m,\nu n}+G_{\mu m,\nu n}$ and $J^s_{\mu m,\nu n}=J_{\mu m,\nu n}-G_{\mu m,\nu n}$. The reader should note that the mapping $G\to -G$ interchanges the c and s variables and amounts to a rotation $\phi_{\mu m}\to\phi_{\mu m}+\pi/2$ of the molecules.

III. MEAN-FIELD CALCULATION

Let us introduce a six-component variable $S_{im}=(c_{1m},c_{2m},c_{3m},s_{1m},s_{2m},s_{3m})$. In Fourier space, the mean field is

$$h_i(\mathbf{q})=\sum_j J_{ij}(\mathbf{q})\langle S_j(\mathbf{q})\rangle, \tag{7}$$

where $J_{ij}(\mathbf{q})$ is a 6×6 block diagonal matrix constructed from the J^c and J^s couplings of Eq. (6):

$$J(\mathbf{q})=\begin{pmatrix} J^c(\mathbf{q}) & 0\\ 0 & J^s(\mathbf{q})\end{pmatrix}. \tag{8}$$

Because there are three columns in the unit cell, the mean-field transverse components of $\mathbf{q}$ are zero (this detailed calculation is not shown here). From now on, without any ambiguity, we replace $\mathbf{q}$ by q, its z component. We also set to unity the intracolumn distance between two molecules ($d_\parallel=1$). The J^c and J^s matrices are then

$$J^{c,s}(q)=\begin{pmatrix} J_\parallel(q) & J^{c,s}_{12} & J^{c,s}_{31}(q)\\ J^{c,s}_{12} & J_\parallel(q) & J^{c,s}_{23}(q)\\ J^{c,s}_{31}(q) & J^{c,s}_{23}(q) & J_\parallel(q)\end{pmatrix}, \tag{9}$$

with

$$\begin{aligned} J_\parallel(q)&=\cos q+J_2\cos 2q,\\ J^c_{12}&=\tfrac{3}{2}(J+G),\\ J^c_{23}(q)&=J^c_{31}(q)=3(J+G)\cos\tfrac{1}{2}q,\\ J^s_{12}&=\tfrac{3}{2}(J-G),\\ J^s_{23}(q)&=J^s_{31}(q)=3(J-G)\cos\tfrac{1}{2}q. \end{aligned} \tag{10}$$

The displacement of the $\mu=3$ columns changes the coordination number from 6 to 3 and adds a $\cos(\frac{1}{2}q)$ factor.

A. Second-order phase transition temperature T_c

Order-disorder continuous phase transitions are related to the divergence of the ''paramagnetic'' susceptibility χ, which in turn is related to the single-site susceptibility $\chi_0=1/2T$, with $k_B=1$, by the standard random-phase approximation relation

$$\chi(q)=\chi_0[\mathbb{1}-\chi_0 J(q)]^{-1}. \tag{11}$$

The 6×6 matrix between square brackets is singular when at least one of its eigenvalues is zero. As the temperature is lowered, the transition occurs for some q_c maximizing one of the six eigenvalues of $J(q)$. The corresponding eigenvector identifies the configuration involved in the transition. The eigenvalue itself is twice the critical temperature T_c.

$J(q)$ is block diagonal, and the sixth-order characteristic equation reduces to the two cubic equations given by

$$\det[J^{c,s}(q)-j^{c,s}\mathbb{1}]=0. \tag{12}$$

The eigenvalues are

$$j^{c,s}_1(q)=J_\parallel(q)-J^{c,s}_{12}, \tag{13a}$$

$$j^{c,s}_2(q)=J_\parallel(q)+\tfrac{1}{2}[J^{c,s}_{12}-\sqrt{J^{c,s2}_{12}+8J^{c,s}_{23}(q)^2}], \tag{13b}$$

$$j^{c,s}_3(q)=J_\parallel(q)+\tfrac{1}{2}[J^{c,s}_{12}+\sqrt{J^{c,s2}_{12}+8J^{c,s}_{23}(q)^2}]. \tag{13c}$$

The eigenvectors are of the form

$$v^{c,s}_1(q)=(1,-1,0), \tag{14a}$$

$$v^{c,s}_2(q)=[j^{c,s}_2-J_\parallel(q),\ j^{c,s}_2-J_\parallel(q),\ 2J^{c,s}_{23}(q)], \tag{14b}$$

$$v^{c,s}_3(q)=[j^{c,s}_3-J_\parallel(q),\ j^{c,s}_3-J_\parallel(q),\ 2J^{c,s}_{23}(q)]. \tag{14c}$$

For each parameter set (J,G,J_2) we numerically find which of the six eigenvalues is maximal and the corresponding q_c. It turns out that the only two eigenvalues to be maximum are j^c_3 and j^s_3. The critical temperature is thus the maximum of the two temperatures

$$\begin{aligned} T^{c,s}_c&=\max(\tfrac{1}{2}j^{c,s}_3)\\ &=\tfrac{1}{2}(\cos q_c+J_2\cos 2q_c)+\tfrac{3}{8}(J\pm G)\\ &\quad+\tfrac{3}{8}|J\pm G|\sqrt{1+32\cos^2\tfrac{1}{2}q_c}. \end{aligned} \tag{15}$$

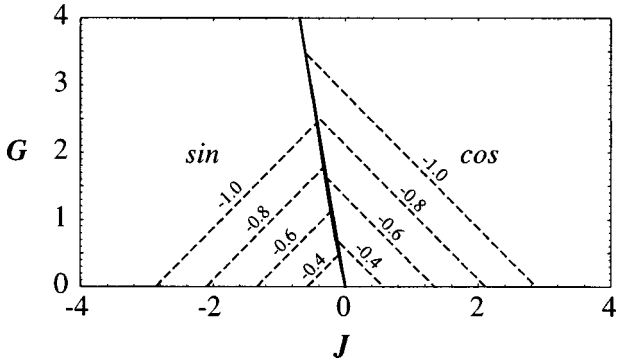

FIG. 2. Phase diagrams at the critical temperature for $J_2=-1.0$, -0.8, -0.6, and -0.4. The full lines, all superimposed with the precision used, are the boundaries between cos and sin phases and the dashed lines are the boundaries between the $q_c=0$ and $q_c\neq 0$ phases. For $G<0$, the diagram is a mirror image of the above with cos and sin phases interverted.

If $T_c^c>T_c^s$ ($T_c^c<T_c^s$), only the cosine (sine) components are involved in the transition. The boundary between the cosine and sine transitions is defined by $T_c^c=T_c^s$. Because of the (a,a,b) structure of the v_3^c and v_3^s eigenvectors, we conclude that columns 1 and 2 play similar roles, whereas column 3 has a distinct behavior.

In the J-G plane and for a particular value of J_2, we identify four regions corresponding roughly to the four quadrants, two of them being shown in Fig. 2. The line $G=0$, where the cosine and sine components are equivalent, is an obvious boundary. The curve

$$|G|=-g(J,J_2)J, \tag{16}$$

on which $T_c^c=T_c^s$, follows from a mechanism similar to the spin-flop mechanism of magnetism. For $|J|$ and $|G|$ sufficiently high relative to $|J_2|$, q_c vanishes, i.e., the transverse couplings have ''untwisted'' the columns. The equation $T_c^c(q_c=0)=T_c^s(q_c=0)$ then relates J and G:

$$(J+G)+|J+G|\sqrt{33}=(J-G)+|J-G|\sqrt{33}. \tag{17}$$

The solutions are $G=0$ and $|G|=-\sqrt{33}J$. Thus, in the limit $q_c=0$, we find $g=\sqrt{33}\approx 5.74$, independently of J or J_2. At $q_c=0$, the columns behave like a single vector flipping under the anisotropic effect of G. For smaller values of $|J|$ and $|G|$, q_c is nonzero and g decreases, but the same mechanism remains.

In the ''cosine'' regions, the helicity at the transition is a function $q_c=q_c(J+G,J_2)$ because $J+G$ is the only combination of J and G appearing in j_3^c. In the ''sine'' regions, we have $q_c=q_c(J-G,J_2)$ for the same reason. For $J_2>-\frac{1}{4}$, q_c vanishes, i.e., each column stabilizes a ''ferromagnetic'' order [16,17]. For $J_2<-\frac{1}{4}$, there is a region of the J-G plane where $q_c\neq 0$, but $q_c=0$ for $|J|$ and $|G|$ high enough. The boundary is determined by the competition between $|J_2|$ and the transverse couplings, respectively, inducing a modulation in the columns and favoring $q_c=0$.

B. Thermal phase diagrams

In order to investigate finite-temperature effects near the order-disorder transition, to better specify the nature of the phases and to rule out the possibility of higher-temperature first-order transitions, we set up a Landau theory from the microscopic model. We follow in essence the method proposed by Bak and von Boehm [20].

1. Free-energy functional expansion

For commodity, we divide the Landau free-energy functional F into two parts: F_T and F_J. In reciprocal space, to fourth order, we find that

$$\begin{aligned}F_T=T\sum_{\mu}\Bigg\{&\sum_{q_1}[c_\mu(q_1)c_\mu(-q_1)+s_\mu(q_1)s_\mu(-q_1)]\\&+\tfrac{1}{4}\sum_{q_1,q_2,q_3}[c_\mu(q_1)c_\mu(q_2)c_\mu(q_3)c_\mu(-q_1-q_2-q_3)\\&+2c_\mu(q_1)c_\mu(q_2)s_\mu(q_3)s_\mu(-q_1-q_2-q_3)\\&+s_\mu(q_1)s_\mu(q_2)s_\mu(q_3)s_\mu(-q_1-q_2-q_3)]\Bigg\},\end{aligned} \tag{18}$$

with $T=1/\beta$. $c_\mu(\tilde{q})$ and $s_\mu(\tilde{q})$ are the Fourier transforms of the mean values $\langle c_{\mu m}\rangle$ and $\langle s_{\mu m}\rangle$. This truncated power expansion is numerically close to the exact value (less than 1% difference) up to $\sqrt{\langle c_{\mu m}\rangle^2+\langle s_{\mu m}\rangle^2}\approx 0.5$. A sixth-order development is 1% accurate up to $\sqrt{\langle c_{\mu m}\rangle^2+\langle s_{\mu m}\rangle^2}\approx 0.65$. For every mean value under this limit of validity, a negligible number of fictitious spins with modulus higher than 1 contribute to the statistics. We also find that

$$\begin{aligned}F_J=-\sum_{\mu,\nu}\sum_{q_1}&[J_{\mu\nu}^c(q_1)c_\mu(q_1)c_\nu(-q_1)\\&+J_{\mu\nu}^s(q_1)s_\mu(q_1)s_\nu(-q_1)].\end{aligned} \tag{19}$$

These expressions represent the free-energy functional for a group of three columns. All the umklapp terms have been dropped from the q summations. These umklapp terms would have pinned the modulation to commensurate values. By ignoring them, we allow incommensurate phases to occupy the entire parameter space, leaving a space of measure zero to commensurate phases. In real systems a devil's staircase [20] is expected instead of the continuous q profile.

2. Order parameters

We then assume that, near the transition, $c_\mu(\tilde{q})=0$ and $s_\mu(\tilde{q})=0$ $(\forall\mu)$ except for $\tilde{q}=\pm q$. In other words, we concentrate on the first harmonic to appear in the modulated phases. This is valid at the transition but it is not excluded that higher harmonics may appear at lower temperatures, as secondary order parameters. $c_\mu(q)$ and $s_\mu(q)$ are the x and y components of three polarization vectors

$$\mathbf{S}_\mu(q)=c_\mu(q)\hat{\mathbf{x}}+s_\mu(q)\hat{\mathbf{y}}. \tag{20}$$

These are complex quantities that may be expressed as

$$c_\mu = |c_\mu| e^{i\varphi_\mu^c}, \quad s_\mu = |s_\mu| e^{i\varphi_\mu^s}. \tag{21}$$

This choice of variables allows for any elliptical polarization and relative global phase for each column. To simplify the notation, we replace $|c_\mu|$ by c_μ and $|s_\mu|$ by s_μ and, to avoid any ambiguity, we make no use of the complex c_μ and s_μ anymore. In real space,

$$\langle \mathbf{S}_{\mu k} \rangle = \tfrac{1}{2}[\mathbf{S}_\mu(q) e^{iqz_k} + \mathbf{S}_\mu^*(q) e^{-iqz_k}] = c_\mu \cos(qz_k + \varphi_\mu^c)\hat{\mathbf{x}} + s_\mu \cos(qz_k + \varphi_\mu^s)\hat{\mathbf{y}}, \tag{22}$$

with $z_k = k + \frac{1}{2}\delta_{\mu 3}$, so that $\varphi_\mu^{c,s}$ are the global phases of the different columns μ at the $z=0$ level.

The function to minimize is then $F = F_T + F_J$, with

$$F_T = T \sum_\mu [2(c_\mu^2 + s_\mu^2) + \tfrac{1}{4}(6(c_\mu^4 + s_\mu^4) + 4\{2 + \cos[2(\varphi_\mu^s - \varphi_\mu^c)]\} c_\mu^2 s_\mu^2)] \tag{23}$$

and

$$F_J = -\sum_{\mu,\nu} [J_{\mu\nu}^c c_\mu c_\nu \cos(\varphi_\nu^c - \varphi_\mu^c) + J_{\mu\nu}^s s_\mu s_\nu \cos(\varphi_\nu^s - \varphi_\mu^s)], \tag{24}$$

with couplings as previously defined. F is a function of c_μ, s_μ, $\varphi_\mu^{c,s}$, and q that is, at first, numerically minimized. The reader should note that the permutation $1 \leftrightarrow 2$ in the indices leaves F unchanged, which reflects the equivalence of columns 1 and 2.

3. Helicity patterns

We numerically observe simple relationships between the phases φ_μ^c and φ_μ^s. These in turn lead to a simplified expression for the free-energy functional. For $G=0$, the cosine and sine components are equivalent and $s_\mu = c_\mu$. By numerically minimizing F we obtain

$$\varphi_\mu^s - \varphi_\mu^c = \pm \frac{\pi}{2}, \tag{25}$$

so that the modulation appearing in the columns is circularly polarized, with a helicity given by the sign on the right-hand side. This sign ($\sigma_\mu = \pm$) may differ from one μ value to another. We denote $(\sigma_1, \sigma_2, \sigma_3)$ the helicity configuration of the three sublattices of columns. For $G=0$, the only allowed helicity configuration is $(+++)$ [or equivalently $(---)$]. Depending on the sign of J, the relative global phases of each component from one column to another are 0 or $\pm\pi$. For $J>0$, the columns adopt a ''ferromagneticlike'' arrangement

$$\varphi_1^{c,s} = \varphi_2^{c,s} = \varphi_3^{c,s}, \tag{26}$$

and for $J<0$, the triangular geometry imposes a colinear ''antiphase''

$$\varphi_1^{c,s} = \varphi_2^{c,s} = \varphi_3^{c,s} \pm \pi. \tag{27}$$

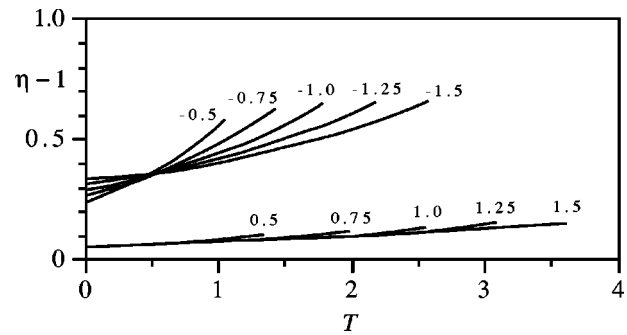

FIG. 3. $\eta(T)$ curves for $G=0$ and different values of J. $\eta(T)$ is defined only for T below the critical temperature T_c, which depends on the J value.

Instead of the ordinary ''120° state'' for an evenly frustrated system, our system concentrates the frustration in the 1-2 bond, which has a lower coordination number than 1-3 and 2-3 bonds. In contrast to the results obtained at $T=0$ in [9], where every column was forced to adopt the same amplitude and a deformed 120° state was achieved, we obtained here a fully colinear antiphase.

This fundamental difference arises from the freedom of the above model to adopt different amplitudes of modulation for the different columns. This was not allowed in [9]. Using the definitions

$$\eta_c = \frac{c_3}{c_1} = \frac{c_3}{c_2}, \quad \eta_s = \frac{s_3}{s_1} = \frac{s_3}{s_2}, \tag{28}$$

we have presented on Fig. 3 η_c and η_s as functions of the temperature, for $G=0$ and different values of J. Because $G=0$, we have $\eta_c = \eta_s = \eta$ and the curves are identical for each J. This ratio has a well-defined value only below the critical temperature T_c. It is to be noticed that for all cases presented, η is always larger than unity. For $J<0$, the behavior is even larger than for $J>0$. As a consequence, the displaced columns show a larger amplitude for the modulated phases.

For $G \neq 0$, the rotational invariance is broken and we expect noncircularly polarized phases. Numerically, we still find $\varphi_\mu^s - \varphi_\mu^c = \pm\pi/2$ and, if $|J| \geqslant |G|$, a $(+++)$ configuration is realized. If $|J| < |G|$, we have a $(++-)$ configuration, as previously found in [12] (see Fig. 4). The intercolumn relative phases are related to the sign of $J+G$ for the cosines and of $J-G$ for the sines. For $J+G>0$,

$$\varphi_1^c = \varphi_2^c = \varphi_3^c, \tag{29}$$

while for $J+G<0$,

$$\varphi_1^c = \varphi_2^c = \varphi_3^c \pm \pi. \tag{30}$$

If G is replaced by $-G$, identical relations hold for φ_μ^s.

These phase relationships divide the J-G plane in four quadrants, as seen in Fig. 4. This diagram possesses an athermal character since these relative phases are the only variables having an influence on the sign of each term of F, $\cos(\frac{1}{2}q)$ being always positive. However, it is important to stress that the phases (and the phase relationships) have a

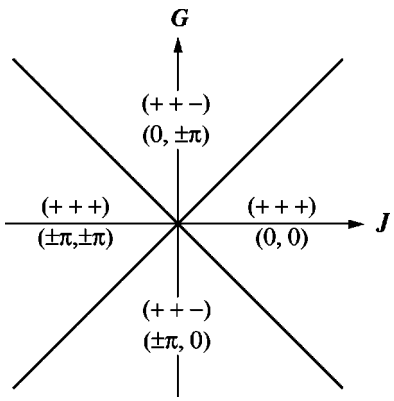

FIG. 4. Helicity patterns and phase differences in the J-G plane. The first number (0 or $\pm\pi$) is the difference $\varphi_3^c-\varphi_1^c$ and the second is $\varphi_3^s-\varphi_1^s$.

physical meaning only when their corresponding amplitudes are nonzero. From these partial results, we may rewrite F in a simpler form

$$F_T=2T\{2c_1^2+c_3^2+2s_1^2+s_3^2+\tfrac{1}{4}[3(2c_1^4+c_3^4+2s_1^4+s_3^4)+2(2c_1^2s_1^2+c_3^2s_3^2)]\}, \tag{31}$$

$$F_J=-(\cos q+J_2\cos 2q)(2c_1^2+c_3^2+2s_1^2+s_3^2)-3(J+G)c_1^2-12|J+G|(\cos\tfrac{1}{2}q)c_1c_3-3(J-G)s_1^2-12|J-G|(\cos\tfrac{1}{2}q)s_1s_3. \tag{32}$$

The absolute values of some couplings reflects the helicity choice made in order to minimize F. The positive signs of the coefficients of $c_1^2s_1^2$ and $c_3^2s_3^2$ favor competition between c and s variables.

4. Phase boundaries at T_c

In this section we investigate the first order-disorder transition to appear when lowering the temperature, that is, the highest temperature for which at least one order parameter is nonzero. This resulting critical temperature and the boundary between different phases should agree with the results found in Sec. III A. This is presented in order to express the consistency of the Landau theory and its numerical treatment. For each parameter set (T,J,G,J_2), we minimize F defined with the expressions (31) and (32); using Eqs. (23) and (24) would be equivalent, but numerically inefficient. The critical temperature is found by selecting T such that one of c_1, c_3, s_1, or s_3 is as small as possible, but nonzero. We have recovered the diagram of Fig. 2, T_c and q_c being identical to those found in Sec. III A. We also conclude that the transitions are always of second order, even with sixth-order terms in the expansion of F_T.

For $q_c=0$, that is, when $|J|$ or $|G|$ is large enough, some analytical results are easily obtainable. The matrix $\{H_F\}_{ij}=\{\partial^2F/\partial x_i\partial x_j\}$, where $\mathbf{x}$ is a vector constructed from the order parameters $[\mathbf{x}=(c_1,c_3,s_1,s_3)]$, defines the local convexity of F. We diagonalize H_F to express this convexity along some eigendirections: h_F, the four eigenvalues of H_F, are the convexity coefficients. For each parameter set (T,J,G,J_2), F is minimal for a particuliar $\mathbf{x}$. For the algebraic form of the present F, the sign of each convexity coefficient at $\mathbf{x}=\mathbf{0}$ indicates whether $\mathbf{0}$ is a minimum or not: F is minimal at $\mathbf{0}$ if every coefficient is positive, but one or more negative coefficients means that $\mathbf{0}$ is no longer a minimum. A vanishing eigenvalue of H_F at $\mathbf{x}=\mathbf{0}$ corresponds to a second-order transition.

H_F has two distinct, doubly degenerate eigenvalues given by

$$h_F^{c,s}=3[2T-(1+J_2)-(J\pm G)]+\sqrt{[2T-(1+J_2)-3(J\pm G)]^2+144(J\pm G)^2}. \tag{33}$$

h_F^c correspond to $J+G$ and h_F^s to $J-G$. For a set (J,G,J_2), T is the critical temperature T_c when every h_F is positive at $\mathbf{x}=\mathbf{0}$, but at least one vanishes. The eigenvalues vanish at the temperatures

$$T_c^{c,s}=\tfrac{1}{2}(1+J_2)+\tfrac{3}{8}(J\pm G)+\tfrac{3}{8}|J\pm G|\sqrt{33}. \tag{34}$$

We retain the solution that keeps T_c positive for any J and G. These expressions coincide with Eq. (15) if $q_c=0$. The cosine or sine components order depending on which of the two temperatures T_c^c or T_c^s is maximum. We have a phase boundary between the two types of order for $T_c^c=T_c^s$. This equality is equivalent to Eq. (17). For $q_c\neq 0$, the same analysis leads easily to Eq. (15).

For a small q_c, we expand $T_c^{c,s}$ in powers of q_c^2. The q_c^4 coefficient is negative. The boundary between $q_c=0$ and $q_c\neq 0$ phases occurs when the q_c^2 coefficient vanishes. We have the relation

$$|J\pm G|=\frac{22}{\sqrt{33}}(-J_2-\tfrac{1}{4}), \tag{35}$$

which defines the boundaries on Fig. 2 (the dashed lines).

5. Thermal phase diagrams

Below the critical temperature and for J and G exactly lying on the $|G|=-g(J,J_2)J$ curve, both the c and s components order. For the same G and J_2 but for a higher J, the c components order first, followed at lower temperature by the s components and conversely for a lower J. Consequently, a concomitant ordering of both the c and s components exists for a range of J. From the equivalence of the $\mu=1$ and $\mu=2$ columns, we have observed that $c_1=c_2$ and $s_1=s_2$. Conversely, because of their mutual hindrance, $c_1<c_3$ and $s_1<s_3$.

We show in Fig. 5 the thermal phase diagrams for constant values of G and $J_2=-1$. The symmetry of F with respect to $G\leftrightarrow -G$ allows us to consider only $G\geqslant 0$. Each diagram has a high-temperature disordered phase (denoted d) and at lower temperatures ordered phases sin and cos. For $q\neq 0$, these phases are denoted M sin and M cos. Just below the $|G|=-g(J,J_2)J$ curve is a mixed sin+cos phase that transforms continuously from sin to cos when approaching this region from large positive and negative J. For $q\neq 0$, the region sin+cos is an elliptical phase denoted E.

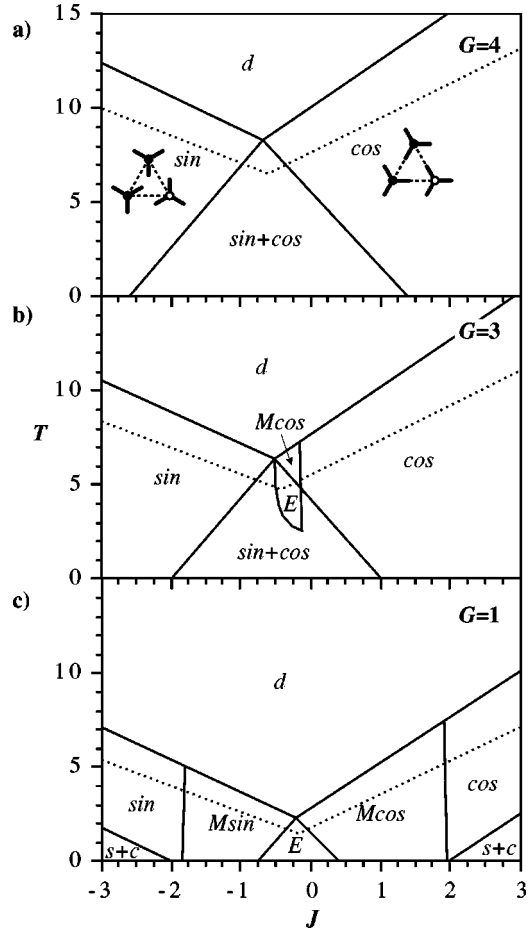

FIG. 5. Thermal phase diagrams for strong transverse couplings (see the text). For (a) $G=4$ there are no modulated phases. For (b) $G=3$ the modulated phases are reentrant. The dotted lines indicate the limit of validity of the fourth-order free-energy expansion, below which at least one order parameter is greater than 0.5. The insets schematically illustrate the orientations of the three molecules in a plaquette for sin and cos phases.

For high values of $|J|$ or $|G|$, q remains zero below T_c, as shown in Fig. 5(a). For small $|G|$ and increasing $|J|$, steep boundaries between modulated and nonmodulated phases are crossed [see Fig. 5(c)]: q vanishes continuously from M cos to cos and from M sin to sin. Inversely, for small $|J|$ and increasing $|G|$, a reentrant boundary is crossed: A modulated elliptical phase reappears with increasing temperatures [see Fig. 5(b)]. For high values of $|J|$, below the critical temperature, the disordered variables (c in the sin phase and s in the cos phase) order at lower temperatures, forming sin+cos phases. For $G=1$ [Fig. 5(c)], we see the beginning of this phase for $|J|\gtrsim 2$. The phase boundaries are parallel to the sin and cos boundaries with the disordered phase. These low-temperature phases are not shown on Figs. 5(a) and 5(b), but they occur respectively for $|J|\gtrsim 6$ and 8. Because helicity configurations have meaning only when c_μ, s_μ, and q are nonzero, that is, for E phases, the diagrams of Fig. 5 do not show the richness of Fig. 4. For the choice of parameters, the central E phases in Fig. 5 are $(++-)$ phases. For smaller values of $|G|$, it is expected that a phase boundary between E phases having $(++-)$ and $(+++)$ configurations would be observable.

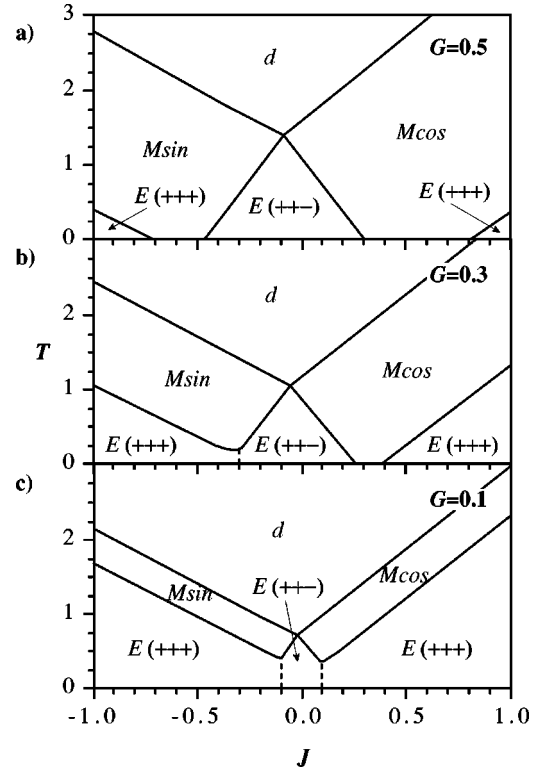

FIG. 6. Thermal phase diagrams in the quasi-one-dimensional regime (see the text). For (a) $G=0.5$ the $E(++-)$ and $E(+++)$ are separated. For (b) $G=0.3$ and (c) $G=0.1$ the dashed lines denote first-order helicity reversal transitions.

Indeed, the quasi-one-dimensional regime, where $|J_1|,|J_2|\gg|J|,|G|$, is interesting because it is more realistic for HHTT, with E phases having different helicity patterns. We show in Fig. 6 thermal phase diagrams for G from 0.1 to 0.5. Both the $E(+++)$ and $E(++-)$ phases exist and are sometimes adjacent. On the J interval presented in Fig. 6, all the ordered phases are modulated. The temperature ''depth'' of the M sin and M cos phases is approximately proportional to $|G|$ and independent of J.

Figure 7 illustrates schematically the positions and orientations of the molecules for different phases encountered in the diagrams of Fig. 6, in the case where $G>0$. Some are also present in Fig. 5. The length of the tails represent the amplitude of ordering. The M sin phase [Fig. 7(a)] shows modulated order with uniform orientations along the columns and where column 3 is in phase opposition. For $G>0$, the M cos phase [Fig. 7(b)] is a modulated ferromagneticlike state. The maximum lengths of the tails shows that column 3 is more ordered than columns 1 and 2. The corresponding sin and cos phases are illustrated in Fig. 5(a). Figure 7(c) and 7(d) represent the various elliptical phases E encountered from left to right in Fig. 6.

IV. MONTE CARLO SIMULATIONS

A. Method and algorithm

We use the Metropolis algorithm (see [21] for general Monte Carlo methods) to simulate a three-dimensional lattice of XY variables. Our goal is to obtain the essential features of the thermal phase diagram of the system (4), restricting

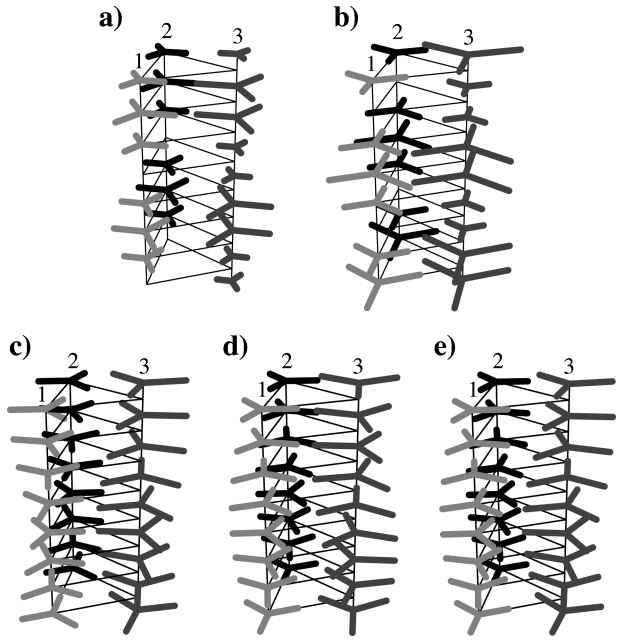

FIG. 7. Schematic illustration of the orientations of molecules and the amplitudes of mean values with $G>0$ for (a) the M sin phase with column 3 in phase opposition, (b) the M cos phase with column 3 in phase conjunction, (c) the $E(+++)(\pi,\pi)$ phase, (d) the $E(++-)(0,\pi)$ phase, and (e) the $E(+++)(0,0)$ phase.

ourselves to the quasi-one-dimensional regime. The above method has been implemented in conjunction with the ''spiraling'' algorithm [22,23], which simulates incommensurate helical phases by relaxing the constraint associated with the finite size of the lattice. Outside the critical regime, the results are in principle independent of the lattice size. This method is applied on each column of N XY variables $\{\phi_1,\ldots,\phi_N\}$. We simulate the neighbors of ϕ_1 and ϕ_2 with *phantom* sites (denoted by a prime) related to sites of the opposite extremity of the column:

$$\phi'_{N-1}=\phi_{N-1}-N\Delta,\quad \phi'_N=\phi_N-N\Delta. \tag{36}$$

For the sites ϕ_{N-1} and ϕ_N, we use the phantom neighbors

$$\phi'_1=\phi_1+N\Delta,\quad \phi'_2=\phi_2+N\Delta. \tag{37}$$

The reader will note that for $\Delta=0$ simple periodic boundary conditions are recovered. Δ is an effective field representing an additional indefinite length of a lattice modulated with a constant pitch. For the system to select its own boundary conditions, we consider Δ as a thermodynamic variable. Each Monte Carlo step of the spiraling algorithm consists in N ordinary trial flips of the ϕ variables, plus a single trial flip of Δ. We modify Δ by a small random angle $\delta\Delta$. In order for the new Δ to be compatible with the above equations, a twist must be imposed on the lattice:

$$\phi_i\leftarrow\phi_i+(i-1)\delta\Delta. \tag{38}$$

The new state has a new total energy and is then tested for acceptance with the Metropolis algorithm. We may compare the spiraling algorithm to a high-order mean-field approximation, where the exact clusters have the size of the finite lattice used in the simulation. Close to a transition, when the correlation length is large relative to the cluster size, this approximation loses some validity.

We simulated a 6×6 triangular lattice of columns, that is, 12 groups of three columns. We used periodic boundary conditions in the plane and the spiraling algorithm in the columns' direction. Each column has its own Δ variable.

For two neighboring columns with nonplanar interactions (J' and G'), the spiraling algorithm introduces some small energy discrepancies. This problem arises from the nonequivalence of some of the couplings at the edges of the lattice. Due to the relatively small energy involved in this boundary effect (especially for a quasi-one-dimensional system), it was neglected.

We identify the different phases with the nonzero values of the Fourier coefficients of wave vector $\tilde{q}$ of the x and y components defined by

$$a^c_\mu(\tilde{q})=\frac{2}{12N}\sum_{(i,j)\in R_\mu}\sum_k \cos\phi_{ijk}\cos\tilde{q}z_k, \tag{39a}$$

$$b^c_\mu(\tilde{q})=\frac{2}{12N}\sum_{(i,j)\in R_\mu}\sum_k \cos\phi_{ijk}\sin\tilde{q}z_k, \tag{39b}$$

$$a^s_\mu(\tilde{q})=\frac{2}{12N}\sum_{(i,j)\in R_\mu}\sum_k \sin\phi_{ijk}\cos\tilde{q}z_k, \tag{39c}$$

$$b^s_\mu(\tilde{q})=\frac{2}{12N}\sum_{(i,j)\in R_\mu}\sum_k \sin\phi_{ijk}\sin\tilde{q}z_k, \tag{39d}$$

with $z_k=k+\frac{1}{2}\delta_{\mu3}$. R_μ represents the sublattice of μ columns and N is the number of sites in each column. Using these coefficients, we construct the order parameters

$$c_\mu(\tilde{q})=\sqrt{a^c_\mu(\tilde{q})^2+b^c_\mu(\tilde{q})^2}, \tag{40a}$$

$$s_\mu(\tilde{q})=\sqrt{a^s_\mu(\tilde{q})^2+b^s_\mu(\tilde{q})^2}. \tag{40b}$$

The $\langle c_\mu(\tilde{q})\rangle$ and $\langle s_\mu(\tilde{q})\rangle$ profiles show a maximum at $\tilde{q}=q_0$ and may show secondary peaks. Indeed, it has been shown [24] that a third harmonic at $q_3=3q_0$ should appear for linearly polarized columns. In our simulations, this third harmonic should be an indication of such a linear polarization. For each wave vector $\tilde{q}$, we also construct the cosines and sines of the relative phases of the columns defined by

$$\cos(\phi^s_\mu-\phi^c_\mu)(\tilde{q})=\frac{a^s_\mu(\tilde{q})a^c_\mu(\tilde{q})+b^s_\mu(\tilde{q})b^c_\mu(\tilde{q})}{s_\mu(\tilde{q})c_\mu(\tilde{q})}, \tag{41a}$$

$$\sin(\phi^s_\mu-\phi^c_\mu)(\tilde{q})=\frac{b^s_\mu(\tilde{q})a^c_\mu(\tilde{q})-a^s_\mu(\tilde{q})b^c_\mu(\tilde{q})}{s_\mu(\tilde{q})c_\mu(\tilde{q})}, \tag{41b}$$

$$\cos(\phi^c_{\mu+1}-\phi^c_\mu)(\tilde{q})=\frac{a^c_{\mu+1}(\tilde{q})a^c_\mu(\tilde{q})+b^c_{\mu+1}(\tilde{q})b^c_\mu(\tilde{q})}{c_{\mu+1}(\tilde{q})c_\mu(\tilde{q})}, \tag{41c}$$

$$\sin(\phi^c_{\mu+1}-\phi^c_\mu)(\tilde{q})=\frac{b^c_{\mu+1}(\tilde{q})a^c_\mu(\tilde{q})-a^c_{\mu+1}(\tilde{q})b^c_\mu(\tilde{q})}{c_{\mu+1}(\tilde{q})c_\mu(\tilde{q})}, \tag{41d}$$

$$\cos(\phi^s_{\mu+1}-\phi^s_\mu)(\tilde{q})=\frac{a^s_{\mu+1}(\tilde{q})a^s_\mu(\tilde{q})+b^s_{\mu+1}(\tilde{q})b^s_\mu(\tilde{q})}{s_{\mu+1}(\tilde{q})s_\mu(\tilde{q})}, \tag{41e}$$

$$\sin(\phi^s_{\mu+1}-\phi^s_\mu)(\tilde{q})=\frac{b^s_{\mu+1}(\tilde{q})a^s_\mu(\tilde{q})-a^s_{\mu+1}(\tilde{q})b^s_\mu(\tilde{q})}{s_{\mu+1}(\tilde{q})s_\mu(\tilde{q})}. \tag{41f}$$

We compare $\langle\cos(\phi^s_\mu-\phi^c_\mu)(q_0)\rangle$ to the mean-field expression $\cos(\phi^s_\mu-\phi^c_\mu)$ and so on for each mean value.

The amplitudes (40) converge relatively fast, but the angular phases (41) converge much more slowly: They are ratios of fluctuating quantities. For some simulations, we are only interested in the $\langle c_\mu(\tilde{q})\rangle$ and $\langle s_\mu(\tilde{q})\rangle$ values and we have simulated only 2000 Monte Carlo steps per site (MCS/S), including 1000 MCS/S for thermalization. N, the number of sites per column, was set to 40. However, many more steps were needed to obtain the relative angular phases (25 000 MCS/S, including 5000 MCS/S to thermalize). In these cases, N was taken to be 12. To improve numerical efficiency, we discretized the ϕ and Δ variables into 256 values from 0 to 2π.

All simulations are done with $G=0.1$ and $J_2=-1$, a quasi-one-dimensional limit. We perform the simulations by gradually decreasing the temperature for each value of J. This allows a greater numerical stability for low-temperature phases and retains the helicity sign $[(++\mp)$ or $(--\pm)]$ for all temperatures.

Preliminary simulations on a single plaquette of three columns were done to compare the spiraling algorithm with periodic boundaries conditions in some reasonable computing time. For $N=40$, simulations using periodic boundaries along columns give very similar results compared to simulations with the spiraling algorithm, except for smaller mean values (because of higher fluctuations) and slightly displaced peaks. However, the difference is pronounced for $N=12$, where the spiraling algorithm broadens the principal peak, while periodic boundaries conditions destroy the whole spectrum.

B. Thermal phase diagrams

Figure 8 shows a typical result for the temperature profiles $\langle c_1(\tilde{q})\rangle$ and $\langle s_1(\tilde{q})\rangle$, from which the thermal phase diagram is reconstructed: Notice that both q_0 and q_3 peaks appear at specific temperatures (q_3 is folded in the $[0,\pi]$ interval). The $\langle c_\mu(\tilde{q})\rangle$ and $\langle s_\mu(\tilde{q})\rangle$ profiles show that, for $J=-0.15$ a decreasing temperature drives the system from the d phase to the M sin phase and finally to the E phase. The critical temperatures are arbitrarily taken to be the points at which the amplitude of the peak is half its maximum value.

The thermal phase diagram is constructed by repeating the simulations for many J values. Figure 9 shows the diagram for $G=0.1$ and $J_2=-1$. We always obtain

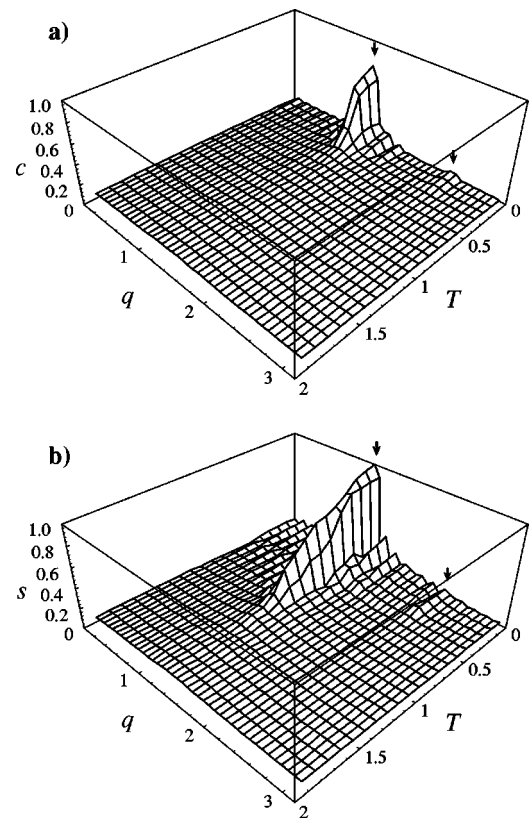

FIG. 8. (a) $\langle c_1(q)\rangle$ and (b) $\langle s_1(q)\rangle$ temperature profiles for $J=-0.15$, $G=0.1$, and $J_2=-1$. The arrows indicate the first and third harmonics. The q_0 peaks appear at $T\approx0.4$ for c_1 and $T\approx0.9$ for s_1.

$\langle\cos(\phi^s_\mu-\phi^c_\mu)(q_0)\rangle\approx0$ and $\langle\sin(\phi^s_\mu-\phi^c_\mu)(q_0)\rangle\approx\pm1$, with signs corresponding to the mean-field helicity configurations: $(++-)$ or $(--+)$ for $|J|<0.1$ and $(+++)$ or $(---)$ for $|J|>0.1$. Some longer simulations were done to establish clearly the phase differences, at $J=-0.15$, -0.05, 0.05, and 0.15. For high enough amplitudes $|\langle c_\mu(q_0)\rangle|$ and $|\langle s_\mu(q_0)\rangle|$, all relative phases are compatible with the mean-field calculations and with the results just cited. Moreover, many short simulations where done on a single plaquette of three col-

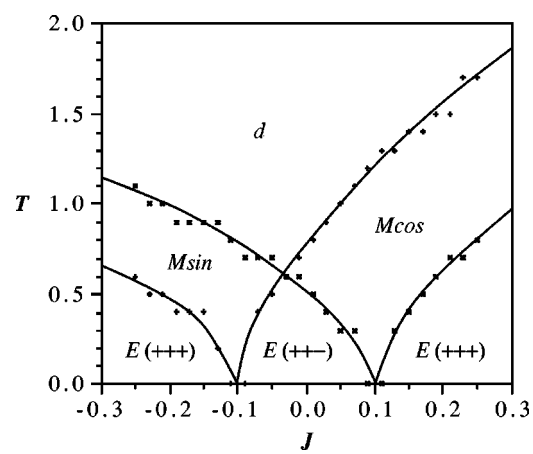

FIG. 9. Thermal phase diagram for $G=0.1$ and $J_2=-1$ from Monte Carlo simulations. The continuous line is a guide to the eye [see Fig. 6(c) for the mean-field diagram].

umns ($N=40$) and, although no phase transition is observed (the system is one dimensional), the phase differences are in excellent agreement with Fig. 4.

Contrary to the mean-field results [Fig. 6(c)], the E phases with different helicity configurations were not found to be adjacent: A linearly polarized phase opens up between the $E(+++)$ and $E(++-)$ phases. On the diagram, for a given value of J, a dot at $T=0$ means that no phase transition was clearly identified when lowering the temperature.

V. DISCUSSION AND CONCLUSION

X-ray measurements on HHTT have lead to the observation of a sequence of phases as temperature is lowered. Two neighboring phases (D_{hd} and H) at intermediate temperatures have a columnar structure. Entering the H phase from the D_{hd} phase involves a mutual and concomitant ordering of both the position and orientation of the molecules along the columns. However, we may assert that the positions of the molecules, being submitted to more stringent intermolecular forces, are rapidly frozen with decreasing temperature, as compared to their orientations. This is the main justification for restricting the model studied in this paper to orientational degrees of freedom. The results obtained and in particular the general trend of the thermal phase diagram should help in understanding the behavior of HHTT inside the H phase.

The first result of interest is the existence of linearly polarized phases at T_c with a finite wave number q_c in the columnar direction, q_c decreasing with increasing values of the intermolecular couplings and eventually vanishes. A similar disappearance of the amplitude modulation has been predicted [9] at $T=0$, where it then shows up as an unwinding of the helical pitch. At T_c, for large $|J|$ and $|G|$, a boundary at a constant slope of magnitude $|G|/J=-\sqrt{33}$ is predicted between two linearly polarized phases. This behavior is reminiscent of the two boundary structures predicted at $T=0$ between linearly polarized phases. At $T=0$, the constant slopes of the boundaries are respectively -3 and -5 [9].

The frustration between ordered columns of molecules with an octupolar moment on a triangular lattice is high. Part of this frustration is relaxed by freezing the positions of the molecules and displacing one of every three columns by half a lattice spacing in the columnar direction. However, even under these conditions, substantial orientational frustration remains for negative values of the interaction parameter J. At $T=0$, with only fixed amplitude phases, a noncollinear distorted 120° phase was obtained with global relative orientation between the columns, which depends only on the pitch of the helical modulation of the columns [9]. In the present case, allowing for a different amplitude on the displaced column compared to the undisplaced ones, the resulting configuration is collinear and the relative orientations (e.g., $\phi_3-\phi_1$) are independent of the pitch. This angular configuration, typical of unfrustrated systems, is achieved only through a larger amplitude of modulation for the displaced columns as compared to the undisplaced ones, as shown in Fig. 3.

For values of G moderate compared to the intracolumnar couplings (Fig. 6) both the helicity patterns $(+++)$ and $(++-)$ are predicted. Also, it is to be noted that the temperature range over which the linearly polarized and modulated phases exist narrows with decreasing values of G. Under these conditions, it is expected that the elliptical phases rapidly appear on lowering the temperature below T_c. In this temperature range and for $|G|>|J|$, an elliptical phase $(++-)$ is predicted. Recall that the $(++-)$ phase is the one observed [5] for HHTT in the H phase. We are then in a position to reiterate that HHTT is a quasi-one-dimensional system where the molecular orientations are determined by the nonrotationally invariant interaction between octupolar moments located on a distorted triangular lattice.

The finite-temperature Monte Carlo simulations on finite-size systems has confirmed the mean-field results. The one important difference is that the $(++-)$ and $(+++)$ configurations are not seen to be adjacent in Monte Carlo simulations, whereas they have a common boundary in the mean-field approximation. The hard-spin constraint $c_{\mu m}^2+s_{\mu m}^2=1$ is automatically satisfied in the Monte Carlo simulations. At low temperature and in the intermediate regime $|J|\approx|G|$, the system is ambivalent between $(+,+,+)$ and $(+,+,-)$ configurations. A modulated linear phase generally implies greater fluctuations in the orientation of each molecule since the mean value $\langle \mathbf{S} \rangle$ is periodically zero. Because the Monte Carlo method implements fluctuations more realistically, it supresses elliptical phases over a finite range of J down to $T=0$, in contrast to the mean-field approximation. This may explain why so few columnar liquid crystal materials have helical phases.

Regarding the $D_{hd}\rightarrow H$ transition in HHTT, this work raises the question of the detailed nature of the observed H phase near the transition: Is there a linearly polarized ''H phase''? The presence of a linearly polarized modulated phase, or even a noncircularly polarized H phase, would be an indication of the chiral octupolar nature of the molecule (the G coupling). Such a linearly polarized phase would automatically have a third harmonic in the modulation of the columns [24], leading to x-ray satellites. The most important result of this paper is the higher amplitude of modulation predicted for the displaced columns compared to the undisplaced columns. This behavior would affect the x-rays results through the Debye-Waller factors, i.e., the relative amplitude (larger amplitude equals smaller fluctuations) of the different Bragg peaks.

ACKNOWLEDGMENTS

The authors are grateful to M. L. Plumer for many discussions. G. L. would like to thank W. M. Saslow for helpful suggestions related to the simulations. This work was supported by NSERC (Canada) and by FCAR (Québec).

[1] S. Chandrasekhar, *Liquids Crystals*, 2nd ed. (Cambridge University Press, Cambridge, 1992).
[2] P.-G. de Gennes and J. Prost, *The Physics of Liquid Crystals*, 2nd ed. (Oxford University Press, New York, 1993).
[3] E. F. Gramsbergen, H. J. Hoving, W. H. de Jeu, K. Praefke, and B. Kohne, Liq. Cryst. **1**, 397 (1986).
[4] G. Yan and T. C. Lubensky, J. Phys. II **7**, 1023 (1997).
[5] E. Fontes, P. A. Heiney, and W. H. de Jeu, Phys. Rev. Lett. **61**, 1202 (1988).
[6] E. Fontes, Ph.D. dissertation, University of Pennsylvania, 1989 (unpublished).
[7] S. Idziak, Ph.D. dissertation, University of Pennsylvania, 1992 (unpublished).
[8] A. Caillé and M. Hébert, Phys. Rev. E **54**, R4544 (1996).
[9] M. Hébert and A. Caillé, Phys. Rev. E **53**, 1714 (1996).
[10] M. Hébert and A. Caillé, Phys. Rev. E **51**, R1651 (1995).
[11] M. Hébert and M. L. Plumer, Phys. Rev. E **54**, 550 (1996).
[12] M. L. Plumer, A. Caillé, and O. Heinonen, Phys. Rev. B **47**, 8479 (1993).
[13] M. Pesquer, M. Cotrait, P. Marsau, and V. Volpilhac, J. Phys. (France) **41**, 1039 (1980).
[14] M. Cotrait, P. Marsau, M. Pesquer, and V. Volpilhac, J. Phys. (France) **43**, 355 (1982).
[15] M. Hébert and A. Caillé, Phys. Rev. B **49**, 55 (1994).
[16] W. Selke, in *Phase Transitions and Critical Phenomena* (Academic, London, 1992), Vol. 15.
[17] S. Redner and H. E. Stanley, Phys. Rev. B **16**, 4901 (1977).
[18] T. Horiguchi and Y. Fukui, Phys. Rev. B **50**, 7140 (1994).
[19] H.-Y. Choi, A. B. Harris, and E. J. Mele, Phys. Rev. B **40**, 3766 (1989).
[20] P. Bak and J. von Boehm, Phys. Rev. B **21**, 5297 (1980).
[21] *Monte Carlo Methods in Statistical Physics*, edited by K. Binder, Topics in Current Physics Vol. 7 (Springer, Berlin, 1979).
[22] W. M. Saslow, M. Gabay, and W.-M. Zhang, Phys. Rev. Lett. **68**, 3627 (1992).
[23] M. Collins and W. M. Saslow, Phys. Rev. B **53**, 8533 (1996).
[24] M. B. Walker, Phys. Rev. B **22**, 1338 (1980).